Original

Nycander, J.; Hieronymus, M.; Roquet, F.:
The nonlinear equation of state of sea water and the global water mass distribution.
In: Geophysical Research Letters. Vol. 42 (2015) 18, 7714 - 7721.
First published online by AGU: 28.09.2015

https://dx.doi.org/10.1002/2015GL065525

AGU PUBLICATIONS

Geophysical Research Letters

RESEARCH LETTER
10.1002/2015GL065525

Key Points:
- The formation of AAIW depends on cabbeling
- The layering of NADW and AABW depends on thermobaricity
- A theory of the water mass distribution must use a nonlinear equation of state

Correspondence to:
J. Nycander,
jonas@misu.su.se

Citation:
Nycander, J., M. Hieronymus, and F. Roquet (2015), The nonlinear equation of state of sea water and the global water mass distribution, *Geophys. Res. Lett.*, *42*, 7714–7721, doi:10.1002/2015GL065525.

Received 25 JUL 2015
Accepted 7 SEP 2015
Accepted article online 10 SEP 2015
Published online 30 SEP 2015

The nonlinear equation of state of sea water and the global water mass distribution

Jonas Nycander[1], Magnus Hieronymus[2], and Fabien Roquet[1]

[1]Department of Meteorology, Bolin Centre for Climate Research, Stockholm University, Stockholm, Sweden, [2]Institute for Coastal Research, Helmholtz Zentrum Geesthacht, Geesthacht, Germany

Abstract The role of nonlinearities of the equation of state (EOS) of seawater for the distribution of water masses in the global ocean is examined through simulations with an ocean general circulation model with various manipulated versions of the EOS. A simulation with a strongly simplified EOS, which contains only two nonlinear terms, still produces a realistic water mass distribution, demonstrating that these two nonlinearities are indeed the essential ones. Further simulations show that each of these two nonlinear terms affects a specific aspect of the water mass distribution: the cabbeling term is crucial for the formation of Antarctic Intermediate Water and the thermobaric term for the layering of North Atlantic Deep Water and Antarctic Bottom Water.

1. Introduction

A vertical hydrographic section through the Atlantic displays the three main water masses of the deep ocean (i.e., below the thermocline): Antarctic Bottom Water (AABW), North Atlantic Deep Water (NADW), and Antarctic Intermediate Water (AAIW) (Figure 1). The salinity field has a complex layered structure, with a salinity maximum at middepth (in the NADW), and salinity minima both below, near the bottom (in the AABW), and above, around 1000 m depth (in the AAIW). What causes this structure?

Traditional explanations focus on the surface forcing. For example, the AAIW might be the result of the downward Ekman pumping at midlatitudes. However, an analysis of recent observational data shows that the wind stress in fact forces upwelling in the density range of AAIW [*Sallée et al.*, 2010]. *Pedlosky* [1992], on the other hand, focused on the upwelling forced by mixing at the base of the thermocline. He showed that if this upwelling is horizontally nonuniform, it may force a layered baroclinic geostrophic velocity structure in the deep ocean below. This would result in layering of the tracer fields. Recently, *Nikurashin and Vallis* [2011, 2012] have proposed a semianalytic model of the overturning and stratification of the deep ocean that shows how the formation of AABW and NADW depends of the surface forcing and the interior mixing. However, both *Pedlosky* [1992] and *Nikurashin and Vallis* [2011, 2012] neglected the influence of salinity and used a linearized equation of state (EOS).

With a linear EOS, the thermal expansion coefficient α and the haline contraction coefficient β are both assumed to be constant, but in reality they are functions of the thermodynamic state variables. In particular, α is a function of temperature (which gives rise to cabbeling) and pressure (the thermobaric effect). These are the two most important nonlinearities.

Here we will show by numerical simulations that the nonlinearities of the EOS are crucial for the global water mass distribution. Instead of varying the forcing or the geometry, as is customary, we will vary the EOS. Specifically, we will demonstrate that the layering of AABW and NADW depends on the thermobaric nonlinearity, and that the formation of AAIW depends on the cabbeling nonlinearity.

2. Simulations

The simulations were done with the ocean general circulation model (OGCM) NEMO 3.2 [*Madec*, 2008] in the ORCA1 configuration, which has a spatially varying horizontal grid resolution of approximately 1°. Our configuration has 46 vertical levels and uses the dynamic ocean ice model LIM2 [*Fichefet and Maqueda*, 1997]. The Gent McWilliams parameterization [*Gent and McWilliams*, 1990] and the Redi isoneutral diffusion [*Redi*, 1982] are used to account for the mixing done by unresolved eddies, with the eddy diffusivity 1000 m^2/s.

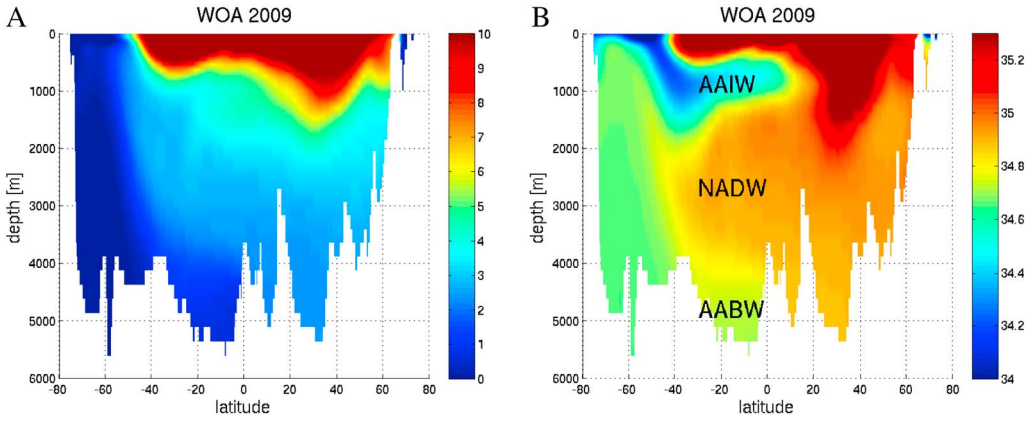

Figure 1. Atlantic sections of (a) potential temperature (°C) and (b) salinity (psu) along the longitude 23.5W from World Ocean Atlas (WOA) 2009. The three main deep water masses are shown on the salinity plot: Antarctic Intermediate Water (AAIW), North Atlantic Deep Water (NADW), and Antarctic Bottom Water (AABW).

The vertical diffusivity is given by the scheme of *Gaspar et al.* [1990], with the minimum value 1.2×10^{-5} m^2/s, and convection is modeled by setting the vertical diffusivity to 100 m^2/s when $N^2 < 10^{-12}$ s^{-2}. The surface forcing was derived from the reanalysis data ERA40, with restoring of the sea surface salinity toward the observed WOA value [*Brodeau et al.*, 2009]. The forcing from 1958 to 1983 was repeated cyclically. More detailed information about the simulations is given by *Hieronymus and Nycander* [2013a]. All simulations were continued at least 500 years, to an approximate steady state.

The standard version of NEMO 3.2 uses EOS 80 [*Jackett and McDougall*, 1995], but we have also used alternative versions of the equation of state. We express the EOS in terms of the buoyancy b, which is the normalized deviation (with reversed sign) of the density ρ from the constant reference density $\rho_0 = 1027$ kg/m^3:

$$b = -\frac{g(\rho - \rho_0)}{\rho_0} \tag{1}$$

In a Boussinesq model like NEMO, the buoyancy is best regarded as a function of potential temperature θ, salinity S, and depth Z (zero at the sea surface and increasing downward), since the fluid equations then conserve energy [*Vallis*, 2006]. The thermal expansion coefficient α and the haline contraction coefficient β are then defined as

$$\alpha = \frac{1}{g}\left.\frac{\partial b}{\partial \theta}\right|_{S,Z} \tag{2}$$

$$\beta = -\frac{1}{g}\left.\frac{\partial b}{\partial S}\right|_{\theta,Z} \tag{3}$$

The buoyancy is a complicated nonlinear function, which is approximated by long algebraic expressions in EOS 80. In some simulations we will instead use a much simpler expression, which only retains the most essential nonlinearities [*Vallis*, 2006]:

$$b = g\left[-\frac{gZ}{c^2} + \alpha_0(1 + \gamma_B Z)(\theta - \theta_0) + \frac{\gamma_C}{2}(\theta - \theta_0)^2 - \beta(S - S_0)\right] \tag{4}$$

where α_0 is the thermal expansion coefficient at the reference state $\theta_0 = 10°C$, $S_0 = 35$ psu, and $Z = 0$. We use the coefficients suggested by *Vallis* [2006]: $\alpha_0 = 1.67 \times 10^{-4}$ K^{-1}, $\gamma_B = 1.1179 \times 10^{-4}$ (Km)$^{-1}$, $\gamma_C = 1 \times 10^{-5}$ K^{-2}, and $\beta = 0.78 \times 10^{-3}$ psu^{-1}. The term $-gZ/c^2$ (where c is the speed of sound) describes the static compressibility. The two important nonlinearities are the thermobaric term proportional to γ_B, which describes the increase of the thermal expansion coefficient with increasing depth, and the cabbeling term proportional to γ_C, which describes the increase of the thermal expansion coefficient with increasing temperature. *Roquet et al.* [2015] have evaluated and implemented a family of EOS with polynomial form in a general ocean circulation model. They found that the simple form (4) is sufficient to simulate a reasonably realistic global circulation.

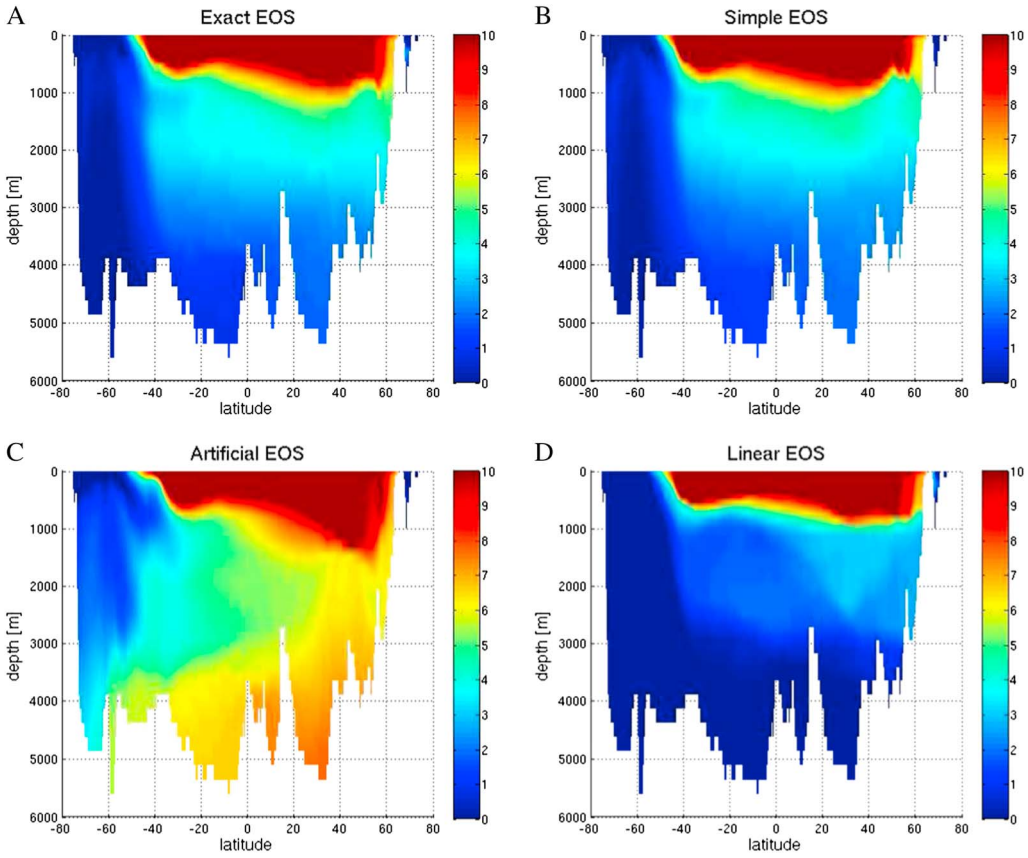

Figure 2. Atlantic sections along −23.5°W of potential temperature (yearly average) at approximate steady state from NEMO simulations using four different equations of state: (a) exact, (b) simple, (c) artificial, and (d) linear.

In order to understand the influence of the nonlinearities of the EOS on the water mass distribution, we have performed simulations with four different versions of the EOS: (a) "exact" the full EOS 80, (b) "simple" the simplified nonlinear EOS defined in equation (4), (c) "artificial" the same as the simplified nonlinear EOS defined in equation (4) but with the opposite sign of the thermobaric coefficient γ_B, (d) "linear" the same as the simplified nonlinear EOS defined in equation (4) but with $\gamma_B = \gamma_C = 0$.

Figure 2 shows Atlantic potential temperature sections from the yearly average of the final state of the four simulations, and Figure 3 shows the corresponding salinity sections. Comparing Figures 1, 2a, and 3a, we see that the simulation with the "exact" EOS reproduces the major deep water masses. The main difference is that the AAIW does not extend as far north in the simulation as in the observations.

A comparison between Figures 2a and 2b and between Figures 3a and 3b, respectively, then shows that using the "simple" EOS in equation (4) gives almost exactly the same water mass distribution as the "exact" EOS. Thus, the thermobaric and cabbeling nonlinearities are indeed the most essential ones, as also found by *Roquet et al.* [2015].

We then compare the simulations with the "simple" and "artificial" versions of the EOS, the only difference being that the latter has opposite sign of the thermobaric coefficient γ_B so that the thermal expansion coefficient decreases with increasing depth. (In the deepest ocean it in fact becomes negative so that an inverted temperature stratification is stable there.) As seen in Figures 2c and 3c this results in a drastically different water mass distribution. With the artificial EOS, the layering between the cold, fresh Antarctic water and the warm, saline North Atlantic water is reversed so that the North Atlantic water is below the Antarctic water. Thus, there is now an Antarctic temperature minimum at middepth instead of an Atlantic salinity maximum.

We also note that the AAIW is virtually unchanged although the thermobaric term has changed sign. Thus, the thermobaric nonlinearity seems to be unimportant for the formation of AAIW.

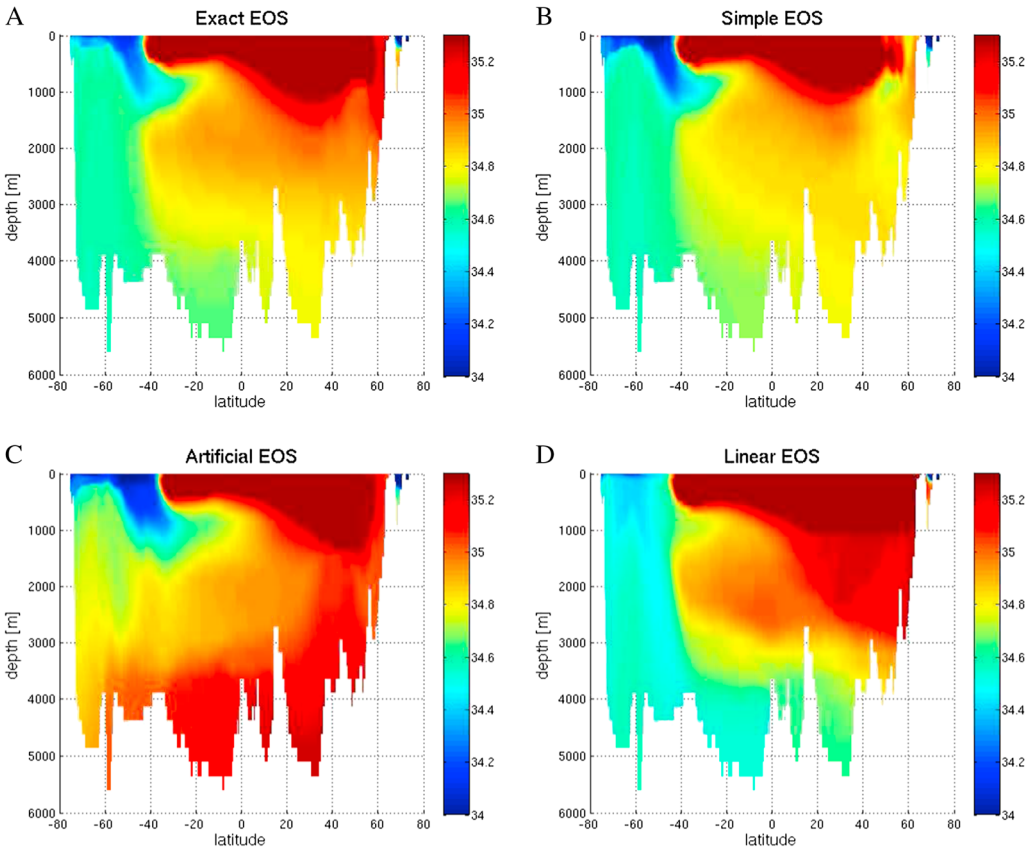

Figure 3. As Figure 2 but for salinity.

The simulation with the "linear" EOS, shown in Figures 2d and 3d, is the only one that does not have the cabbeling nonlinearity, and we see that the main difference is that there is much less AAIW. This is even more striking in the Indian and Pacific Oceans, where the salinity minimum associated with AAIW vanishes entirely when using the linear EOS, as will be seen below. Thus, the cabbeling nonlinearity is crucial for the formation of AAIW.

3. Analysis

The effect of the thermobaric nonlinearity on the deep water mass distribution can easily be understood. Suppose that an Antarctic and a North Atlantic water parcel have the same density when they are situated near the sea surface. If the two parcels are then displaced adiabatically downward, they will no longer have the same density as each other because of thermobaricity. In the real world, and with the "simple" EOS, the density of the colder and fresher Antarctic parcel will increase more rapidly with increasing depth than that of the North Atlantic parcel. (This mechanism was invoked by *Killworth* [1977] to explain how plumes of dense water from the Weddell Sea can reach the foot of the continental slope, arguing that without thermobaricity, the plumes would reach equilibrium far above the bottom.) With the "artificial" EOS, on the other hand, the density of the North Atlantic parcel will increase more rapidly with increasing depth. At large depths the North Atlantic water is therefore denser than the Antarctic water, which explains the reversed layering.

The crucial role of the thermobaric effect for the layering between NADW and AABW has been noted before. For example, *Lynn and Reid* [1968] pointed out that on a plot of σ_0 (the surface-referenced potential density, which does not account for the thermobaric effect) on a vertical section in the western Atlantic, the NADW appears to be partly denser than the AABW.

The effects of the cabbeling nonlinearity on the water mass distribution are more subtle. Because of this nonlinearity, the ratio α/β varies strongly with temperature. At surface pressure and $\theta = 18°C$ this ratio is about 0.3 K^{-1}/psu^{-1}. It then decreases with decreasing temperature, to 0.1 K^{-1}/psu^{-1} at $\theta = 2°C$ and 0.03 K^{-1}/psu^{-1}

at $\theta = -0.8$°C. Therefore, the density stratification is mostly controlled by temperature in warm waters but by salinity in the cold waters south of the Antarctic Circumpolar Current (ACC), where the winter temperature is generally below 2°C.

This makes it possible for the temperature stratification to be inverted south of the ACC, with the coldest water near the surface. This cold and fresh surface layer is formed by precipitation and ice import. Below, there is a temperature maximum in the Upper Circumpolar Deep Water. (In the deepest waters, the ratio α/β is larger because of the thermobaric nonlinearity, and the temperature stratification is stable.) North of the ACC, on the other hand, the salinity decreases with depth, which is compensated by decreasing temperature, as is seen in Figures 1, 2a, and 3a.

Convection and mixed layers deeper than 200–300 m occur in a few locations in the far south, where AABW is formed because of brine rejection during ice freezing, and also between the salinity and temperature dominated regions, near the ACC, where the density stratification is weak. This is where AAIW is formed.

With a linear equation of state (i.e., without the cabbeling nonlinearity), the density is everywhere dominated by temperature. Convection and very deep mixed layers then occur throughout the region south of the ACC, as seen in Figures 2d and 3d. This leads to strong formation of cold bottom water but very little AAIW.

The cabbeling nonlinearity also has another effect that is crucial for the formation of AAIW. When two water parcels with different temperature are mixed, the average density of the two parcels increases, i.e., the mixing creates a density source (or buoyancy sink). This effect is usually referred to as "cabbeling". In the thermocline near the ACC, where the cold and fresh Antarctic water from the south meets the warm and saline Atlantic water from the north, there are strong isopycnal gradients of potential temperature and salinity. Additionally, the isopycnal surfaces at the ACC are very steep, which gives rise to baroclinic instability and strong mixing along these surfaces. The resulting isopycnal heat flux is directed southward and upward and is strong enough to dominate the global vertical heat flux in the depth range 200–2000 m [*Hieronymus and Nycander*, 2013a]. The isopycnal mixing also results in strong cabbeling and hence a strong sink of buoyancy, which dominates the global buoyancy budget in much of the same depth range [*Hieronymus and Nycander*, 2013b]. We suggest that the resulting density increase allows the water to sink irreversibly through the isopycnal surfaces, thus creating AAIW.

This process can be seen in detail in Figure 4, which shows curves of constant salinity and potential density σ_0 on three vertical sections in the Southern Ocean from the simulations with the "exact" and "linear" EOS. Sections are shown both from the Atlantic, at 23.5°W, the Indian Ocean, at 90.5°E, and the Pacific, at 159.5°W. The sections in Figure 4 are from September, i.e., late winter in the Southern Ocean and therefore also approximately show the maximum depth of the mixed layer. We see that the deepest mixed layers occur just north of the region where AAIW is formed.

The isohaline curves with the "exact" EOS in Figure 4 show the signature of a narrow region of downwelling water through the density surfaces around the latitude 50°S and down to 1000 m depth. From there the water flows northward as AAIW. Notice, in particular, how the downwelling water crosses the isopycnal 1027.4 kg/m^3. With the linear EOS this is absent. In the Atlantic section there is still a salinity minimum around 1000 m depth with the linear EOS (though much weaker than with the exact EOS), but in the Indian and Pacific Oceans it has disappeared entirely.

In principle, it would be better to plot neutral density than σ_0 [*McDougall*, 1987], but the σ_0 surfaces do not deviate much from the neutral surfaces over the depth range 0–1000 m relevant for the AAIW. Using the reference depth 500 m would be an even better approximation, but we have checked that both 500 m and 1000 m give essentially the same picture as shown here. We chose to show σ_0 to facilitate comparison with other studies.

Detailed plots similar to those in Figure 4 but for the "simple" and "artificial" EOS also show a distinct signature of downwelling AAIW, similarly as for the "exact" EOS.

We also investigate the volume flux of AAIW by integrating the vertical transport (due to the resolved velocity) across that part of fixed depth surfaces where the potential density is larger than a prescribed value σ_0. Figure 5 shows this transport as a function of σ_0 for four different depths. The curves may be viewed as horizontal sections through the density-depth stream function defined by *Nycander et al.* [2007].

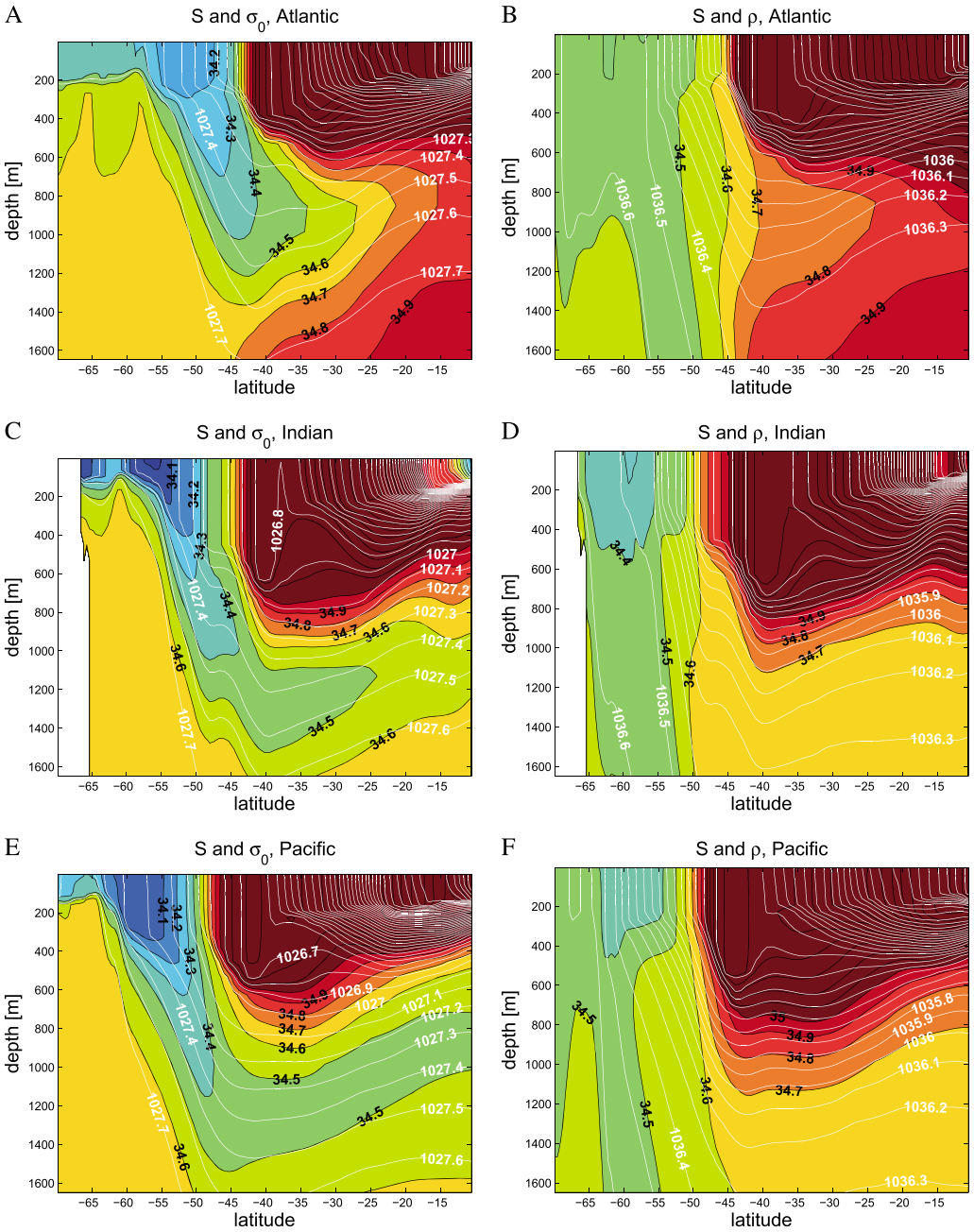

Figure 4. Sections in the Southern Ocean of salinity (colors) and potential density σ_0 (white curves) in September from NEMO simulations. (a, c, and e) Exact EOS. (b, d, and f) Linear EOS. (Figures 4a and 4b) Atlantic (23.5°W). (Figures 4c and 4d) Indian Ocean (90.5°E). (Figures 4e and 4f) Pacific (159.5°W). The contour interval is 0.1 kg/m^3 for potential density and 0.1 psu for salinity (the color scale saturates at 35 psu). With the "exact" EOS the salinity field shows the signature of a narrow region of downwelling low-salinity water that crosses isopycnals.

The largest density at fixed depths occurs near Antarctica, which is thus at the right end of the plots. As we follow the curves leftward, toward lower density, there is first a downward flux, corresponding to the formation of AABW. With the "linear" EOS this is more than 10 Sv (sverdrups), but with the "exact" EOS it is only 5–6 Sv. Then there is strong wind-driven upwelling of up to 30 Sv with the "exact" EOS and up to 40 Sv with the "linear" EOS. With the "linear" EOS this is followed by downwelling starting at densities between 1035.5 (at 577 m depth) and 1036 (at 916 m). With the "exact" EOS there is an additional narrow region with around 5 Sv of downwelling in the density range 1027.2–1027.5 kg/m^3, which corresponds to AAIW, as seen in Figure 4. This downwelling water is indicated by the arrows in Figure 5, and it is absent with the "linear" EOS. Notice that the

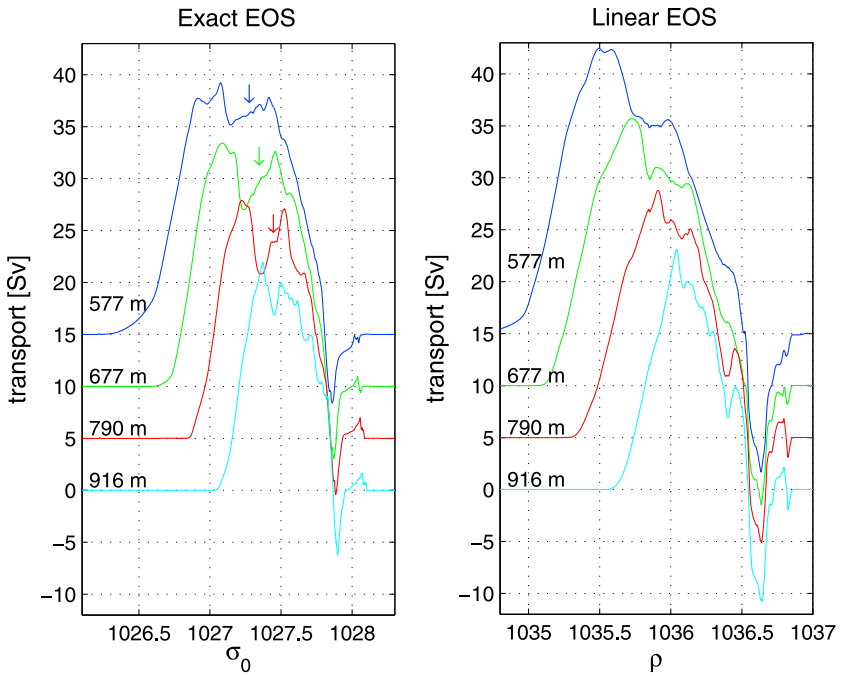

Figure 5. Global vertical volume transport across specified depth surfaces (at 577 m, 677 m, 790 m, and 916 m) with density larger than the value on the horizontal axis. (left) Exact EOS and (right) linear EOS. The curves from successive depths are offset vertically by 5 sverdrups. The arrows indicate the downwelling water in the density range of AAIW.

density of the downwelling water increases slightly with increasing depth, confirming that the downwelling water in Figure 4 crosses isopycnals.

The transport calculations shown in Figure 5 are global and therefore also contain contributions from the Northern Hemisphere. However, we have checked that the region in the Southern Ocean near the ACC dominates in the density range relevant for AAIW.

We conclude that the buoyancy sink due to cabbeling causes downwelling of around 5 Sv of AAIW. This conclusion is supported by other estimates of the water mass transformation due to cabbeling. In simulations with an isopycnal model, *Marsh* [2000] found that cabbeling causes a diapycnal volume flux of up to 7 Sv across the isopycnal surface $\sigma_0 = 27.4$. *Iudicone et al.* [2008] speculated that cabbeling was the main source of the 5–10 Sv of diapycnal transport of AAIW that they calculated in a model with the resolution 2°. Likewise, *Urakawa and Hasumi* [2012] found that cabbeling causes a diapycnal flux of 7 Sv into AAIW in an eddy-permitting simulation of the Southern Ocean. In a diagnostic calculation using the constant isopycnal diffusivity 1000 m^2/s, *Klocker and McDougall* [2010] found that cabbeling causes 2 Sv of diapycnal transport when using the WOCE climatology and 4 Sv when using the temperature and salinity fields from simulations with the circulation model MOM4. There is also observational support for the importance of cabbeling. *Carter et al.* [2014] used hydrographic data to estimate the fractions of the various waters that mix together to form AAIW and concluded that this mixing results in a density increase of up to 0.03 kg/m^3 due to cabbeling, with the maximum at 700 m depth.

In a diagnostic calculation using observed hydrography and parameterized spatially varying diffusivities, *Hieronymus* [2014] found that thermobaricity contributes even more than cabbeling to the boyancy sink at the ACC. Similarly, *Klocker and McDougall* [2010] found that the diapycnal transport due to thermobaricity is larger than that due to cabbeling. Nevertheless, in our simulations the downwelling of AAIW is seen to depend on cabbeling rather than thermobaricity.

4. Summary

By simulating the ocean circulation with an OGCM using different versions of the equation of state (EOS), we have examined the effect of cabbeling and thermobaricity on the water mass distribution of the global ocean. We first confirmed that replacing the full EOS (EOS 80 in our case) by a very simple EOS, with only two

nonlinear terms, does not change the distribution of the three main deep water masses: NADW, AABW, and AAIW [see also *Roquet et al.*, 2015]. The two terms are the cabbeling nonlinearity (the increase of the thermal expansion coefficient α with increasing temperature) and the thermobaric nonlinearity (the increase of α with increasing pressure).

By manipulating these two nonlinearities separately, we then studied their role for the global water mass distribution. When we switched the sign of the thermobaric nonlinearity, the layering of NADW and AABW was reversed, with the Antarctic water situated above the deep water formed in the North Atlantic. Thus, the thermobaric nonlinearity is crucial for the layering of these deep water masses.

Manipulating the thermobaric nonlinearity did not affect the AAIW, but when we linearized the EOS, thus shutting off cabbeling, the AAIW almost vanished. Thus, the cabbeling nonlinearity is crucial for the formation of AAIW.

Acknowledgments
This work was supported by the Swedish Research Council, grant 2008-4400. We are grateful to Johan Nilsson and Kristofer Döös for their useful discussions. The NEMO ocean model is freely available at www.nemo-ocean.eu, and the ORCA1 configuration is available at archive.noc.ac.uk/nemo/. The modified source code files with different versions of the equation of state and the input files necessary to reproduce the experiments are available from the authors upon request (hieronymus.magnus@gmail.com).

The Editor thanks Trevor McDougall and two anonymous reviewers for their assistance in evaluating this paper.

References

Brodeau, L., B. Barnier, A. M. Treguier, T. Penduff, and S. Gulev (2009), An ERA40-based atmospheric forcing for global ocean circulation models, *Ocean Modell.*, *31*, 88–104.

Carter, B. R., L. D. Talley, and A. G. Dickson (2014), Mixing and remineralization in waters detrained from the surface into Subantarctic Mode Water and Antarctic Intermediate Water in the southeastern Pacific, *J. Geophys. Res. Oceans*, *119*, 4001–4028, doi:10.1002/2013JC009355.

Fichefet, T., and M. M. Maqueda (1997), Sensitivity of a global sea ice model to the treatment of ice thermodynamics and dynamics, *J. Geophys. Res.*, *102*, 609–646.

Gaspar, P., Y. Grégoris, and J.-M. Lefevre (1990), A simple eddy kinetic energy model for simulations of the oceanic vertical mixing: Tests at station Papa and long-term upper ocean study site, *J. Geophys. Res.*, *95*, 16,179–16,193.

Gent, P. R., and J. C. McWilliams (1990), Isopycnal mixing in ocean circulation models, *J. Phys. Oceanogr.*, *20*, 150–155.

Hieronymus, M. (2014), A note on the influence of spatially varying diffusivities on the evolution of buoyancy with a nonlinear equation of state, *J. Phys. Oceanogr.*, *44*, 3255–3261.

Hieronymus, M., and J. Nycander (2013a), The budgets of heat and salinity in NEMO, *Ocean Modell.*, *67*, 28–38.

Hieronymus, M., and J. Nycander (2013b), The buoyancy budget with a nonlinear equation of state, *J. Phys. Oceanogr.*, *43*(1), 176–186.

Iudicone, D., G. Madec, B. Blanke, and S. Speich (2008), The role of Southern Ocean surface forcings and mixing in the global conveyor, *J. Phys. Oceanogr.*, *38*, 1377–1400.

Jackett, D. R., and T. J. McDougall (1995), Minimal adjustment of hydrographic profiles to achieve static stability, *J. Atmos. Oceanic Technol.*, *12*(2), 381–389, doi:10.1175/1520-0426(1995)012<0381:MAOHPT>2.0.CO;2.

Killworth, P. D. (1977), Mixing on the Weddell Sea continental slope, *Deep Sea Res.*, *24*, 427–448.

Klocker, A., and T. J. McDougall (2010), Influence of the nonlinear equation of state on global estimates of dianeutral advection and diffusion, *J. Phys. Oceanogr.*, *40*, 1690–1709.

Lynn, R. J., and J. L. Reid (1968), Characteristics and circulation of deep and abyssal waters, *Deep Sea Res.*, *15*, 577–598.

Madec, G. (2008), Nemo ocean engine. [Available at www.nemo-ocean.eu.]

Marsh, R. (2000), Cabbeling due to isopycnal mixing in isopycnic coordinate models, *J. Phys. Oceanogr.*, *30*, 1757–1775.

McDougall, T. J. (1987), Neutral surfaces, *J. Phys. Oceanogr.*, *17*, 1950–1964.

Nikurashin, M., and G. Vallis (2011), A theory of deep stratification and overturning circulation in the ocean, *J. Phys. Oceanogr.*, *41*, 485–502.

Nikurashin, M., and G. Vallis (2012), A theory of the interhemispheric meridional overturning circulation and associated stratification, *J. Phys. Oceanogr.*, *42*, 1652–1667.

Nycander, J., J. Nilsson, K. Döös, and G. Broström (2007), Thermodynamic analysis of ocean circulation, *J. Phys. Oceanogr.*, *110*, 2038–2052.

Pedlosky, J. (1992), The baroclinic structure of the abyssal circulation, *J. Phys. Oceanogr.*, *22*, 652–659.

Redi, M. H. (1982), Oceanic isopycnal mixing by coordinate rotation, *J. Phys. Oceanogr.*, *12*, 1154–1158.

Roquet, F., G. Madec, L. Brodeau, and J. Nycander (2015), Defining a simplified yet 'realistic' equation of state for seawater, *J. Phys. Oceanogr.*, doi:10.1175/JPO-D-15-0080.1, in press.

Sallée, J.-B., K. Speer, S. Rintoul, and S. Wijffels (2010), Southern Ocean thermocline ventilation, *J. Phys. Oceanogr.*, *40*, 509–529.

Urakawa, L. S., and H. Hasumi (2012), Eddy-resolving model estimate of the cabbeling effect on the water-mass transformation in the Southern Ocean, *J. Phys. Oceanogr.*, *42*, 1288–1302.

Vallis, G. K. (2006), *Atmospheric and Oceanic Fluid Dynamics*, 745 pp., Cambridge Univ. Press, Cambridge, U. K.